THE JOURNAL OF PHYSICAL CHEMISTRY C
A JOURNAL OF THE AMERICAN CHEMICAL SOCIETY

pubs.acs.org/JPCC Article

Investigation of Unusual Conductivity Behavior and Ion Dynamics in Hexamethylguanidinium Bis(fluorosulfonyl)imide-Based Electrolytes for Sodium Batteries

Published as part of The Journal of Physical Chemistry virtual special issue "Advanced Characterization by Solid-State NMR and In Situ Technology".

Karolina Biernacka, Faezeh Makhlooghiazad, Ivan Popov, Haijin Zhu, Jean-Noël Chotard, Craig M. Forsyth, Ruhamah Yunis, Luke A. O'Dell, Alexei P. Sokolov, Jennifer M. Pringle, and Maria Forsyth*

Cite This: https://doi.org/10.1021/acs.jpcc.1c01777 Read Online

ABSTRACT: The development of nonflammable, chemically and thermally stable electrolytes that can replace current organic electrolytes will support improved and safer energy storage technologies. Organic ionic plastic crystals (OIPCs) and their salt mixtures are promising solid-state candidates for battery applications. In this work, the hexamethylguanidinium bis(fluorosulfonyl)imide ([HMG][FSI]) OIPC is investigated in the context of sodium batteries, where sodium bis(fluorosulfonyl)imide (NaFSI) salt is mixed with the OIPC to enhance the ionic conductivity. The thermal behavior of the neat OIPC and the effect of sodium salt addition were investigated by differential scanning calorimetry (DSC). Broadband dielectric spectroscopy (BDS) experiments, along with electrochemical impedance spectroscopy (EIS) used to study ion conductivity, showed this system to have unusual temperature-dependent conductivity behavior in comparison to other OIPC systems. The conductivity measured in phase II was higher during the heating cycle compared to that measured upon cooling. Solid-state nuclear magnetic resonance (NMR) spectroscopy combined with XRD and modeling was used to investigate the molecular origin of this behavior. This behavior was also observed in the OIPC containing 5 mol % NaFSI. Pulsed field gradient nuclear magnetic resonance spectroscopy (PFG-NMR) combined with line width analysis was used to examine the ion dynamics. The $[HMG]^+$ cation has almost a 2 orders of magnitude lower diffusion coefficient relative to the $[FSI]^-$ anion, and combined with the very narrow ^{23}Na line width, it appears that the dynamics of the two latter ions are decoupled from the larger $[HMG]^+$ cation, suggesting the possibility of high Na^+ transport in this electrolyte. Our study contributes to the fundamental understanding of dynamics in OIPC-based solid electrolytes for sodium batteries and highlights the complexity and importance of external parameters such as the thermal history of the material properties.

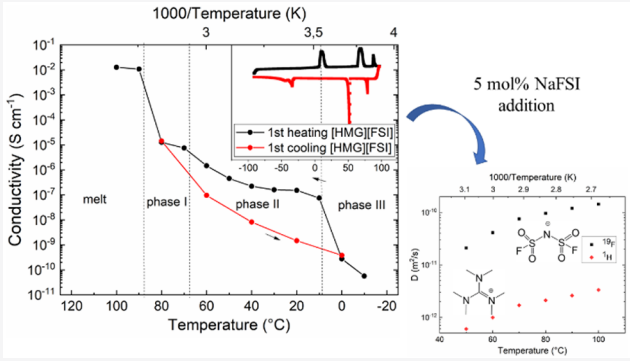

■ INTRODUCTION

OIPCs are a unique class of solid-state electrolyte materials that are increasingly drawing attention due to their negligible volatility and increased safety in contrast to that of electrolytes based on organic flammable solvents that are typically used in electrochemical cells.[1−3] Moreover, many OIPCs are characterized by high thermal and electrochemical stability that makes them good candidates for electrochemical device applications.[4,5] The term plastic arises from their ability to deform under stress without fracture, and this property typically coincides with a high degree of ionic mobility/diffusivity linked with the intrinsic structural disorder and dynamics and enhanced mechanical stability.[6]

Because of a large number of potential cation/anion combinations, it is possible to adjust not only the chemical and thermal properties of OIPCs but also their electrolyte performance. Ion conduction in these materials can occur through either vacancies in the lattice or extended defects such as dislocations or grain boundaries.[7,8] Unfortunately, the

Received: February 26, 2021
Revised: April 21, 2021

complex relationships between the structures of the constituent ions and important material properties such as ionic conductivity and phase behavior are still not fully understood; therefore, more research on new OIPCs needs to be conducted to further develop electrolyte materials with the thermal, electrochemical, and transport properties required to support efficient sodium battery performance. Encouragingly, it was observed that introducing new species (e.g., doping the OIPC with Li or Na salt as needed for battery operation) can increase the ionic conductivity.[9−11] Another phenomenon which has a significant influence on the conductivity values is the occurrence of solid−solid phase transitions. With increasing temperature, OIPCs typically undergo solid−solid phase transitions, resulting in increased local disorder as a result of the onset of rotational and/or translational ion dynamics. These changes typically facilitate increased ion transport.[12] Phase I, which is the most "plastic" and conductive phase, by definition occurs just below the melting point.

So far, most of the reported studies on the effects of doping OIPCs with salts have focused on the use of Li salts for applications in Li batteries.[11,13,14] The use of OIPCs for Na devices is still in its infancy. The first study of OIPCs with sodium salt mixtures was reported by Forsyth et al., who investigated the phase behavior of the OIPC *N*-methyl-*N*-ethyl-pyrrolidinium bis(trifluoromethanesulfonyl)amide ([C_2mpyr][TFSI]), upon mixing with sodium salt NaTFSI.[15] Unfortunately, the ion conduction in these materials was relatively low, reaching 3×10^{-4} S cm^{-1} for 40 mol % NaTFSI at 60 °C. Moreover, an increase in conductivity was not observed upon further sodium salt addition, as was previously reported for lithium systems, showing the difference in material properties depending on the target ions incorporated into the electrolyte system. Subsequently, the same research group investigated *N*,*N*-dimethyl-pyrrolidinium dicyanamide ([C_1mpyr][$N(CN)_2$]) mixed with Na[$N(CN)_2$] at concentrations from 5 to 50 mol %. Again, no significant conductivity increase upon Na salt addition was observed, and phase separation occurred.[16] To improve the ionic conductivity, higher sodium salt compositions were studied using trimethyl-(isobutyl)phosphonium bis(trifluoromethanesulfonyl)amide ([P_{111i4}][TFSI]) organic ionic plastic, and sodium metal electrochemistry was demonstrated.[17] Recently, an OIPC based on another small phosphonium cation, triisobutyl-(methyl)phosphonium ([P_{1i444}]), combined with the bis-(fluorosulfonyl)imide (FSI) anion, was mixed with various sodium salts (NaFSI, NaTFSI, and $NaPF_6$) to investigate mixed anion effects.[18,19] However, all of the reported electrolyte mixtures were characterized by low melting temperatures, preventing them from solid-state sodium battery applications at ambient temperature. Recently, [C_2mpyr][FSI] was studied for sodium-based battery applications, but the addition of various amounts of NaFSI resulted in liquid electrolytes.[20]

The effect of the anion and cation on the physicochemical properties of various phosphonium-based OIPCs ([P_{1i444}][FSI], [P_{1i444}][TFSI], and [P_{111i4}][TFSI]) mixed with the sodium salt of the same anion has been investigated.[21] The properties of these electrolytes varied significantly depending on the sizes of the anion and cation, which demonstrated the general idea of possible correlations between the chemistry and size of the ionic species in the OIPCs and the resulting phase behavior and transport in these materials. However, there is still a long way to go to develop strategies to design such OIPC-based electrolytes with optimum behavior in terms of mechanical stability, high conductivity, and high Na^+ transport number, so more research on OIPC-based electrolytes needs to be conducted.

New OIPC materials have recently been prepared on the basis of novel organic cations, with the aim of further controlling the melting points and plastic phase behavior over a wide temperature range and enhancing the conductivity and electrochemical stability.[22−25] Previous work on lithium electrolyte systems based on the new OIPC, hexamethylguanidinium bis(fluorosulfonyl)imide ([HMG][FSI]), showed promising properties (good transport properties and reversible deposition and stripping of lithium).[26] However, the effect on this OIPC of adding sodium salt is yet to be investigated. In this work, we focus on understanding the molecular-level behavior of pure [HMG][FSI] and the effects of adding a low concentration of sodium salt (NaFSI) on the material properties. The thermal phase behavior, structural changes, ion conductivity, and dynamics of 5 mol % NaFSI and the neat OIPC were studied by utilizing differential scanning calorimetry (DSC), synchrotron X-ray diffraction (SXRD), electrochemical impedance spectroscopy (EIS), broadband dielectric spectroscopy (BDS), and solid-state nuclear magnetic resonance (NMR) spectroscopy.

METHODS

Synthesis of Electrolyte Materials. Acetonitrile (≥99.9%, Merck Milipore Australia) and sodium bis(fluorosulfonyl)imide (NaFSI) (>99.9%, Coors tek US) were purchased commercially and used as received. Neat OIPC hexamethylguanidinium bis(fluoromethanesulfonyl)imide, [$((CH_3)_2N)_3C$][FSI], was synthesized following our previously reported procedure.[27] Electrolytes in this work were prepared in an argon-filled glovebox by directly mixing appropriate amounts of sodium salt and neat [HMG][FSI] in various molar ratios. The mixtures were dissolved in dry acetonitrile, which was removed by 48 h of high-vacuum drying on a Schlenk line (24 h at room temperature followed by 24 h at 50 °C).[28] As a result, electrolytes were prepared: x mol % NaFSI $(100 - x)$ mol % [HMG][FSI].

Differential Scanning Calorimetry (DSC). In this work, the Mettler Toledo differential scanning calorimeter system was used. All samples were prepared in a glovebox under an argon atmosphere. Vacuum-dried samples of 5−15 mg mass were weighed and hermetically sealed in an aluminum pan. An empty aluminum pan was used as a reference. All samples were first cooled to −95 °C before heating to 100 or 200 °C (various temperatures were used due to the concentration effects on thermal decomposition) and kept at the highest temperature for 30 min. The cooling and heating rate was 10 °C/min. The onsets of the endothermic peaks were used to determine the solid−solid phase-transition temperature (T_{s-s}) and the melting temperatures (T_m).

Synchrotron XRD. Variable-temperature synchrotron X-ray powder diffraction (XRD) on neat [HMG][FSI] was performed at the Australian Synchrotron, powder diffraction beamline. The material was packed and sealed in 0.3 mm borosilicate glass capillaries (product of Charles Super Company, Natick, MA, USA) in an Ar-filled glovebox. The samples were then cooled using an Oxford Cryosystems cryostream, which can be heated with a Cyberstar hot-air blower to up to 80 K. For this experiment, the wavelength was set at 0.827 Å with a zero shift of ±0.006° using a Si(111)

https://doi.org/10.1021/acs.jpcc.1c01777
J. Phys. Chem. C XXXX, XXX, XXX−XXX

double-crystal monochromator before data acquisition. The ramp rate and equilibration time used for the experiment were 2 °C/min and 5 min, respectively. An array of 16 MYTHEN ID microstrip silicon detectors with each module spanning about 5° in 2θ covered data collection over the angular range from 2 to 76°. The data were collected at temperatures chosen according to different phases of the plastic crystal for 20 s at two detector settings. The data collected from both detectors were merged for each measurement using the Pdviper software, and the results were plotted and analyzed. The observed reflections were indexed using DICVOL,[29] and full pattern matching was performed using the Fullprof Suite Program.[30,31] A total of 14 parameters were refined, including the cell parameters, the sample shift, and the profile function (pseudo-Voigt).

Single-Crystal XRD. Single-crystal X-ray diffraction data were obtained from a colorless prismatic crystal with approximate dimensions of 0.261 × 0.165 × 0.085 mm^3 at 10 °C using a Rigaku Synergy S diffractometer with Cu Kα radiation (α = 1.54184). Clear, well-defined diffraction intensities were observed and were integrated and corrected for Lorentz polarization and absorption effects using CrysAlisPro 1.171.40.53.[32] The crystal structure was solved and refined by standard methods using the SHELX-2018 software suite.[33] The [HMG][FSI] ion pair was modeled with both the cation and anion disordered over crystallographic inversion centers, thus ASU comprised a half-occupancy $[HMG]^+$ cation and $[FSI]^-$ anion. Because of the extensive disorder in both the HMG cation and the FSI anion, least-squares restraints were applied to the final refinement cycles such that equivalent S−N, S−O, and S−F distances were restrained to be similar (command in refinement program SHELXL - SADI). Overall, the anisotropic displacement parameters of all atoms were relatively large, and for some of the F and O atoms, these parameters were restrained to approximate isotropic behavior (command ISOR). After the completion of the data collection, the above crystal specimen was slowly cooled (at ca. 1 K/min) to −50 °C. However, the resulting diffraction images showed very poor diffraction peaks only at low angles, and the observed pattern could not be indexed.

Conductivity Measurements. The ionic conductivity was measured for the neat OIPC and its mixtures with sodium salt using by two complementary techniques: electrochemical impedance spectroscopy (EIS) and broadband dielectric spectroscopy (BDS). EIS experiments were performed by applying an AC potential to the electrochemical cell and then measuring the impedance as a function of frequency. All of the EIS measurements were performed on a MTZ-35 impedance analyzer (Bio-Logic Science Instruments, France) equipped with a Eurotherm 2204 temperature controller. Samples were packed in a glovebox under an argon atmosphere into a home-designed conductivity cell (a dip cell), which consists of two platinum electrodes. The dip cell was put into a specially designed brass block, which was heated using a cartridge heater connected to a Eurotherm 2204e temperature controller. Cooling of the dip cell was achieved with liquid nitrogen and vermiculite insulation. The conductivity measurements were repeated on duplicate samples. A temperature range of 30−100 °C with 10 °C intervals was used for all experiments. The samples were equilibrated for 30 min at each temperature. The frequency range applied was from 1 MHz to 50 mHz.

Broadband dielectric spectroscopy (BDS) is an alternative form of impedance spectroscopy. An external electric field of fixed or changing frequency is applied to polarize dipoles inside the material, and the response of the system is measured. BDS, in contrast to standard EIS, operates with the frequency-dependent complex parameters characterizing the properties of the studied material, such as complex dielectric permittivity or complex conductivity. Conductivity measurements were performed using an Alpha-A analyzer from Novocontrol in the frequency range of 10^{-1} to 10^6 Hz. Upper and bottom electrodes in the cell were separated by a cap assuring a fixed electrode distance of 0.4 mm and a diameter of 10.2 mm during the measurements. The samples were placed between the electrodes and measured with a voltage amplitude of 0.1 V. A Quatro temperature controller (Novocontrol) was used for variable-temperature measurements. The samples were stabilized for 20 min at each temperature to an accuracy of within ±0.2 °C. The temperature protocol used was as follows: two scans from −40 to 100 °C conducted twice, followed by two scans from 30−100 °C, with 10 °C intervals for heating cycles and 20 °C intervals for cooling.

Solid-State Nuclear Magnetic Resonance (Solid-State NMR). Static ^1H, ^{23}Na, and ^{19}F NMR spectra were recorded on a Bruker Avance III 11.7 T wide-bore solid-state spectrometer (500 MHz) with either a magic angle spinning (MAS) 4 mm probe or a static 5 mm HX extended temperature range probe. Samples were packed into either 4 mm MAS rotors or 5 mm glass tubes in an argon atmosphere glovebox. The spectra were recorded and analyzed using Topspin software. Single-pulse excitation was used for ^1H and ^{23}Na while a Hahn echo pulse sequence was used for ^{19}F. Gaussian/Lorentzian functions (or a CSA line shape in the case of ^{19}F) were used to fit the curves and to calculate the peak widths (full width at half-maximum, fwhm) to study the mobility of ions. To investigate in more detail the local structures and dynamics within the materials at different phases, measurements were performed at temperatures ranging from −60 to 100 °C, with a minimum waiting period of 10 min for the sample to reach a stable temperature.

Pulsed-Field Gradient Nuclear Magnetic Resonance (PFG-NMR). The diffusivities of the $[HMG]^+$ cation and $[FSI]^-$ anion were determined by ^1H and ^{19}F pulse-field gradient stimulated echo (PFG-STE) NMR for 5 mol % NaFSI in [HMG][FSI]. The measurement was performed on a Bruker Avance III 300 MHz spectrometer equipped with a diff50 probe. The data was recorded every 10 °C over the 20 to 100 °C temperature range and analyzed with Topspin. All samples were prepared according to the preparation method in the previous section.

^{19}F NMR Parameter Calculations. ^{19}F chemical shielding anisotropy (CSA) parameters were calculated from the crystal structure using the CASTEP software[34] running in the Materials Studio environment. A fully ordered crystal structure was first specified by arbitrarily selecting one cation conformation. The positions of the hydrogen atoms were optimized with the lattice parameters, and other atomic coordinates were fixed. NMR parameters were then calculated from this structure using revised Perdew, Burke, and Ernzerhof functionals, a plane wave basis set cutoff of 550 eV, eight k-space points sampled, and ultrasoft pseudopotentials.

https://doi.org/10.1021/acs.jpcc.1c01777
J. Phys. Chem. C XXXX, XXX, XXX−XXX

■ RESULTS

Neat [HMG][FSI]. *Thermal Phase Behavior.* The thermal phase behavior of the neat [HMG][FSI] was evaluated by differential scanning calorimetry (DSC). The measured melting temperature of the neat OIPC was 87 °C, which is in agreement with the literature.[27]

As can be seen from Figure 1, three endothermic transitions were observed: peaks at 8 and 67 °C in the heating scan are

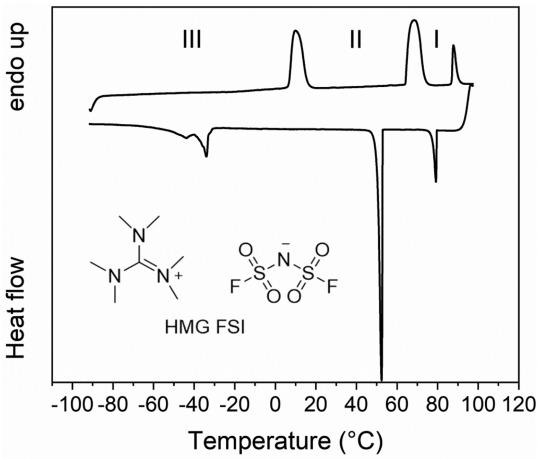

Figure 1. DSC heating traces for neat [HMG][FSI] recorded on second heating (top) and cooling (bottom) scans.

assigned to the solid−solid phase transition from phase III to phase II and the subsequent transition to phase I, respectively. The third peak at the highest temperature (87 °C) corresponds to the melting transition. This melting transition is characterized by the lowest entropy of fusion equal to 7 J mol^{-1} K^{-1}, demonstrating the existence of significant motional degrees of freedom in phase I. This entropy of fusion is lower than, for example, that of [Pyr5][TFSI] (*N*,*N*′-trimethylene pyrazolium bis(trifluoromethanesulfonyl)imide) or [C_2epyr][FSI] (*N*,*N*-diethylpyrrolidinium bis(fluorosulfonyl)imide), for which entropies of melting are equal to 15.8 and 9 J mol^{-1} K^{-1} respectively.[28,35] Moreover, this low value means that the material meets Timmerman's criterion of <20 J K^{-1} mol^{-1} for plastic crystal behavior.[36] Small entropies of fusion arise from the rotational disorder of the species inside the long-range-ordered structure.[14] The thermal behavior of OIPCs depends on the nature and size of their cations and anions and their interaction. In general, FSI^--based OIPCs exhibit lower entropy of melting due to higher disorder structure compared to that of other types of anions such as $TFSI^-$ and also [C_2epyr][FSI] (9 J mol^{-1} K^{-1}), [C_2mpyr][FSI] (10 J mol^{-1} K^{-1}), and [N_{1222}][FSI] (8 J mol^{-1} K^{-1}). Similarly, [HMG][FSI] consisting of a bulky cation with extensive charge delocalization together with the FSI anion, resulting in lower Coulombic interactions presenting a lower entropy of fusion (7 J mol^{-1} K^{-1}).

After melting, the sample was cooled, and on the cooling DSC curve (Figure 1, bottom trace), three crystallization peaks were observed. Each of the crystallization peaks corresponds to a solid−solid phase transition, from phase I to II, II to III, and the structural transition of the sample from phase III. The peak recorded at the lowest temperature of ∼−25 °C indicates multiple events that may indicate the complex and sluggish nature of the solid−solid phase transition (phase II to III). It suggests difficulty in forming the most thermodynamically stable crystal structure, which might be explained by a possible supercooling effect before crystallization. To investigate this behavior in more detail, the experiments described in the following sections were performed.

Synchrotron XRD. Synchrotron X-ray diffraction (SXRD) and single-crystal diffraction were used to investigate the crystal structures and acquire further information on the phase transitions observed by DSC.

Figure 2 shows synchrotron diffraction patterns between 4 and 25° in 2θ recorded at various temperatures for the neat

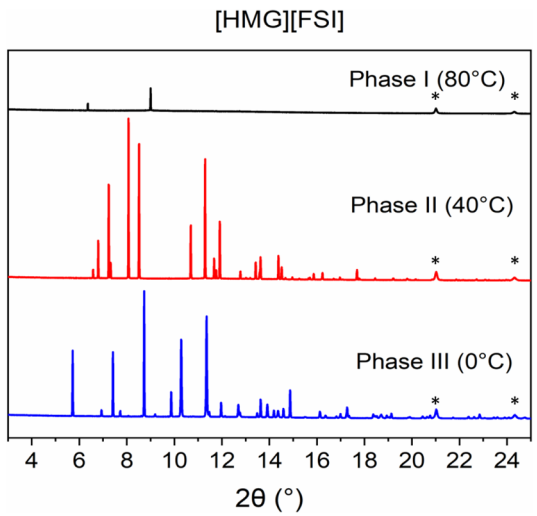

Figure 2. Synchrotron XRD patterns for neat [HMG][FSI] in phase III at 0 °C, phase II at 40 °C, and phase I at 80 °C.

[HMG][FSI]. The temperatures at which the experiments were performed were chosen on the basis of the DSC results, with SXRD patterns recorded before and after each solid−solid phase transition. A secondary cubic face-centered phase was detected in all of the powder patterns measured. The corresponding peaks are highlighted with an asterisk in Figure 2. The powder patterns are typical of plastic crystal materials with intense diffracted peaks at low 2θ but less intense peaks at higher 2θ. Very weak peaks are observed above 25° (2θ) due to the high mobility of the ionic species.

The temperature-dependence study revealed three distinct crystal structures consistent with the DSC measurement and previous studies.[27] As can be seen in Figure 2, the high-temperature phase (phase I at 80 °C) shows only two peaks at low 2θ angles (6.36 and 9.00°, respectively), demonstrating a reduction in long-range periodicity due to the mobility of the HMG cations and FSI anions. On the other hand, phases II and III show a much higher crystallinity, and attempts to solve the crystal structure could thus be performed.

Regarding phase II, single-crystal diffraction data was first obtained at 10 °C (i.e., just above the phase transition from phase III to II). Phase II crystallizes in a triclinic unit cell. It is worth mentioning that due to the mobility of the ions it can be very challenging to solve the complete crystal structure of OIPCs. Two different models can be used to describe this structure. In model 1, both the [HMG] and the [FSI] anions are fully disordered (occupancy = 50%) around the inversion symmetry (−1) of this crystal structure. In model 2, the inversion symmetry is removed (space group *P*1) and each atom is fully occupied, but the displacement parameters are

https://doi.org/10.1021/acs.jpcc.1c01777
J. Phys. Chem. C XXXX, XXX, XXX−XXX

abnormally high to account for the huge mobility. We choose to use model 1 in this report. (See Tables 1 and 2 for complete crystal structure data.)

Table 1. Single-Crystal XRD Refinements for [HMG][FSI] Phase II

empirical formula	$C_7H_{18}F_2N_4O_4S_2$
formula weight	324.37
temperature	283(2) K
wavelength	1.54184 Å
crystal system, space group	triclinic, $P\bar{1}$
unit cell dimensions	a = 7.3042(5) Å, α = 114.849(7)°
	b = 7.3316(5) Å, β = 100.295(6)°
	c = 8.2612(7) Å, γ = 99.836(5)°
volume	379.70(5) Å^3
Z, calculated density	1, 1.419 g/cm^3
absorption coefficient	3.552 mm^{-1}
F(000)	170
crystal size	0.261 × 0.165 × 0.085 mm
θ range for data collection	6.150 to 77.464°
limiting indices	$-8 \le h \le 9$, $-9 \le k \le 7$, $-10 \le l \le 10$
reflections collected/unique	7615/1561 [R(int) = 0.0641]
completeness to θ = 67.684	99.4%
absorption correction	Semiempirical from equivalents
max. and min. transmissions	1.00000 and 0.72656
refinement method	full-matrix least-squares on F^2
data/restraints/parameters	1561/33/173
goodness of fit on F^2	1.160
final R indices [$I > 2\theta(I)$]	$R1$ = 0.0907, $wR2$ = 0.2701
R indices (all data)	$R1$ = 0.1019, $wR2$ = 0.2968
extinction coefficient	0.035(13)
largest diff. peak and hole	0.342 and −0.220 e Å^3

Table 2. Atomic Coordinates (× 10^4) and Equivalent Isotropic Displacement Parameters (Å^2 × 10^3) for [HMG][FSI] Measured at 10 °C[a]

atom	x	y	z	U(eq)
F(1)	9853(9)	493(17)	3555(13)	114(1)
O(2)	9070(30)	2344(18)	4535(17)	242(6)
O(1)	11 774(13)	1240(40)	3960(30)	283(9)
N(1)	8940(30)	−360(20)	1756(17)	265(7)
N(2)	5503(10)	4957(14)	8554(9)	129(2)
N(3)	5715(11)	4085(11)	10 879(11)	121(2)
N(4)	3774(9)	6175(10)	10 661(9)	122(2)
C(1)	9241(17)	−1001(17)	4326(15)	193(5)
C(2)	5040(50)	4860(40)	10 150(30)	85(3)
C(3)	5940(40)	6600(50)	8080(40)	168(8)
C(4)	5830(50)	3140(50)	7160(40)	145(7)
C(5)	7760(40)	3760(50)	11 090(50)	163(9)
C(6)	4660(40)	3030(50)	11 720(40)	153(6)
C(7)	3960(50)	7430(50)	12 540(40)	158(8)
F(2)	2230(30)	6150(50)	9350(40)	150(7)
O(4)	10 570(20)	1290(20)	7784(17)	256(6)
O(3)	12 095(12)	−950(20)	6460(20)	188(4)
S(2)	9050(20)	−2410(20)	6210(20)	243(6)

[a] U(eq) is defined as one-third of the trace of the orthogonalized U_{ij} Tensor.

Model 1 was then used as a starting point for refining the SXRD pattern of phase II at 25 and 40 °C using the Fullprof software.[31] The resulting profile matching at 25 °C is shown in Figure 3. Cell parameters and reliability factors are given in Table 3. As can be seen in Figure S2, the evolution of the cell volume over temperature follows Vegard's law.[37] Work is still in progress to find the best crystallographic description of phase II of this OIPC.

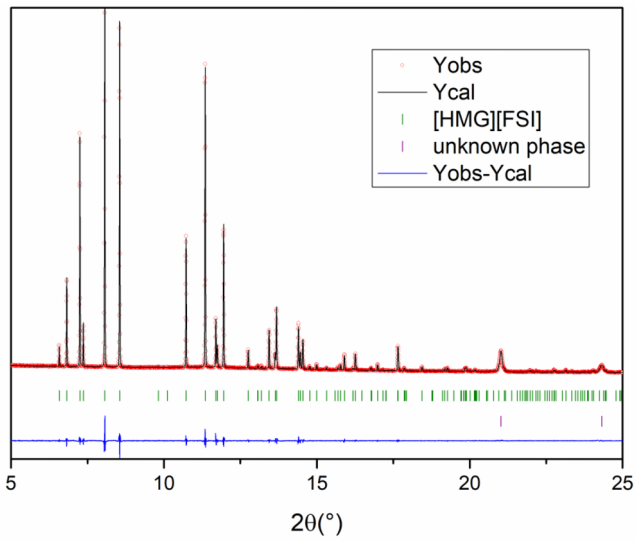

Figure 3. Profile matching of [HMG][FSI] phase II measured at 25 °C. The red dots correspond to experimental data, the black line is the calculated fit, and the blue line is the difference between calculated and observed patterns. The vertical green and purple sticks represent the expected positions of Bragg peaks for [HMG][FSI] and the unknown phase, respectively.

Finally, low-temperature phase III has also been investigated by SXRD. Here again, solving the crystal structure is challenging, and the indexing of the unit cell did not lead to fully satisfactory results. Further temperature-controlled single-crystal diffraction experiments are planned to solve this issue. Nevertheless, our preliminary results show that phase III could be indexed in a 4 times larger unit cell (ca. 1428 Å^3), leading to a V/Z of 357 Å^3, consistent with V/Z = 380 Å^3 in phase II at 10 °C (where Z = 1). This increase in Z (from 1 to 4) reflects a reduction in the orientational and/or rotational disorder in the OIPC upon decreasing temperature that has been previously observed for other OIPCs.[13,16,38]

Conductivity Behavior. The temperature-dependent ionic conductivity exhibits a general trend in which all conductivity values increase steadily with increasing temperature, as seen in Figure 4. Moreover, passing through certain solid−solid phase transitions results in a conductivity "jump" which is attributed to the onset of rotational, orientational, and translational motions of molecules and results in higher disorder and faster ion dynamics. This is typical conductivity behavior for OIPCs and has already been observed in several systems.[21,39] The most significant conductivity increases appear during the transition from phase III to II and during the melting transition, as would be expected. This observation is consistent with the SXRD patterns and XRD data which show that the crystal structure and ion orientations significantly change during the phase III to II transition. Moreover, in phase II the conductivity dependence looks like a polynomial function, which was reported previously by Abu-Lebdeh et al. for a pyrazolium-based organic plastic crystal.[39]

https://doi.org/10.1021/acs.jpcc.1c01777
J. Phys. Chem. C XXXX, XXX, XXX−XXX

Table 3. Summary of the Crystallographic Data for [HMG][FSI] Measured at 25 and 40 °C as Deduced from Profile Matching of SXRD

[HMG][FSI] − phase II − 25 °C			
space group $P\bar{1}$	χ^2 = 2.75	R_p = 12.7%	V = 382.771(3) Å^3
a = 7.33079(3) Å	b = 7.36912(3) Å	c = 8.24663(3) Å	
α = 114.7920(2)°	β = 100.0742(2)°	γ = 99.9658(2)°	
[HMG][FSI] − phase II − 40 °C			
space group $P\bar{1}$	χ^2 = 2.91	R_p = 12.7%	V = 385.450(3) Å^3
a = 7.35084(3) Å	b = 7.40582(3) Å	c = 8.22892(3) Å	
α = 114.7193(2)°	β = 99.8597(2)°	γ = 100.0487(2)°	

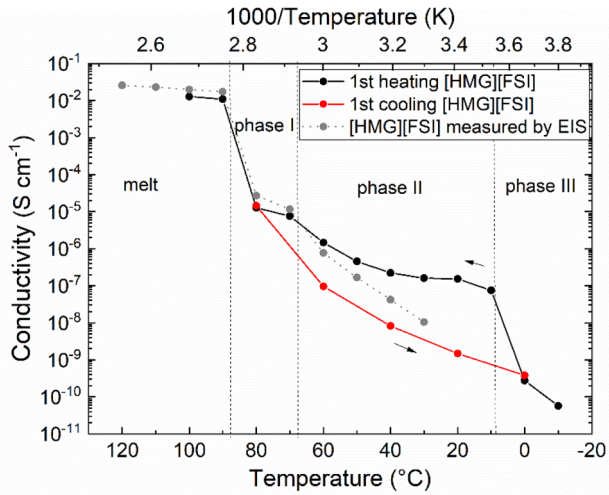

Figure 4. Ionic conductivities of neat [HMG][FSI] recorded during the first heating and cooling cycle measured by BDS (solid lines) and second heating measured by EIS (dotted lines). The dashed lines indicate solid−solid and melting transitions determined by DSC. Each solid phase is labeled with Roman numerals.

Furthermore, the conductivity behavior depends on the thermal history and the heating and cooling cycle, which is in consistent with DSC measurements. The EIS data were recorded at 30 °C, and the values were collected during a second heating scan of the sample to eliminate thermal history effects coming from the material preparation and ensure good mechanical contact between electrodes by melting and recrystallizing the sample. In phase II, the EIS conductivity values recorded during a heating cycle lie between the BDS values recorded on cooling and heating. This may be understood in terms of the thermal history of the sample and the lack of residual effects of the transition from phase III. (See below for further discussion.)

Solid-State NMR Spectroscopy. The structural behavior and the dynamic behavior of [HMG][FSI] in the different phases were studied by variable-temperature static solid-state NMR. Measurements were performed for ^{1}H and ^{19}F nuclei at various temperatures (in the range of −40 to 100 °C), which correspond to different thermal phases of the material. Moreover, to investigate metastability and to help understand the thermal behavior and ion conductivity results, spectra were recorded on both cooling and heating cycles. Each of the nuclei was used to probe a different ion in the OIPC: ^{1}H NMR was used to study the $[HMG]^+$ cation, and ^{19}F was used to study the $[FSI]^-$ anion.

Figure 5 shows spin−echo ^{19}F NMR spectra recorded for [HMG][FSI] at different temperatures during heating (Figure 5a) followed by cooling (Figure 5b). Significant changes in the chemical shielding anisotropy (CSA) powder pattern line shapes can be observed as the material undergoes solid−solid phase transitions. Upon the transition from phase III to II, the ^{19}F line changed dramatically from a CSA pattern with large isotropy (δ_{iso}) and small asymmetry (η) to a CSA with reduced isotropy (δ_{iso}) but increased asymmetry (η). The reduced δ_{iso} suggests increased anion dynamics, while the increased η suggests a major structural rearrangement upon the phase transition. It is found that rotating the sample in the magnetic field resulted in a significant change in the ^{19}F NMR line shapes, as shown in Figure 5c. This confirms the fact that bulky crystals have formed during the cooling process, leading to insufficient power averaging and consequently angular dependency of the CSA pattern.

Furthermore, as the material undergoes solid−solid phase transitions with increasing temperature, a significant increase in anion dynamics can be seen from the ^{19}F NMR spectrum recorded in phase I (at 80 °C, just before the melt) which appears as a single narrow peak, confirming the isotropic rotational dynamics (and potentially also translational mobility) of the anions in phase I.

The crystal structure of phase II was modified to remove the inherent structural disorder by choosing a single anion conformation, and then the ^{19}F CSA parameters were calculated using DFT. The resulting predicted ^{19}F CSA pattern is shown in Figure 5d. Interestingly, this pattern very closely matches the experimentally measured ^{19}F spectrum obtained from phase III at −60 °C rather than that of phase II. This suggests that the anions in phase II are undergoing a dynamic mode that partially averages their ^{19}F CSA pattern while the anions in phase III are static.

Addition of Na Salt. *Thermal Phase Behavior after Sodium Salt Addition to [HMG][FSI].* Figure 6a presents a comparison of DSC thermograms of neat [HMG][FSI] with 2, 5, and 10 mol % NaFSI in [HMG][FSI] and pure NaFSI. Sodium salt addition to [HMG][FSI] significantly changes the thermal behavior. The mixtures are characterized by a lower temperature and a broader and asymmetric melting peak, which overlaps with a solid−solid phase-transition peak. Sodium salt addition depressed the OIPC melting sufficiently that original phase I disappears as the melt transition merges with the II−I transition peak. Moreover, a new endothermic peak appears at 44 °C and grows with increasing Na salt concentration, which may be assigned to the eutectic transition as has been observed before for other OIPCs with sodium and/or lithium salt mixtures.[13,16,21] The broadening of the melting peak and its shift toward lower temperatures relative to the neat OIPC and NaFSI can be explained by the fact that each substance acts as an impurity within the other (sodium

https://doi.org/10.1021/acs.jpcc.1c01777
J. Phys. Chem. C XXXX, XXX, XXX−XXX

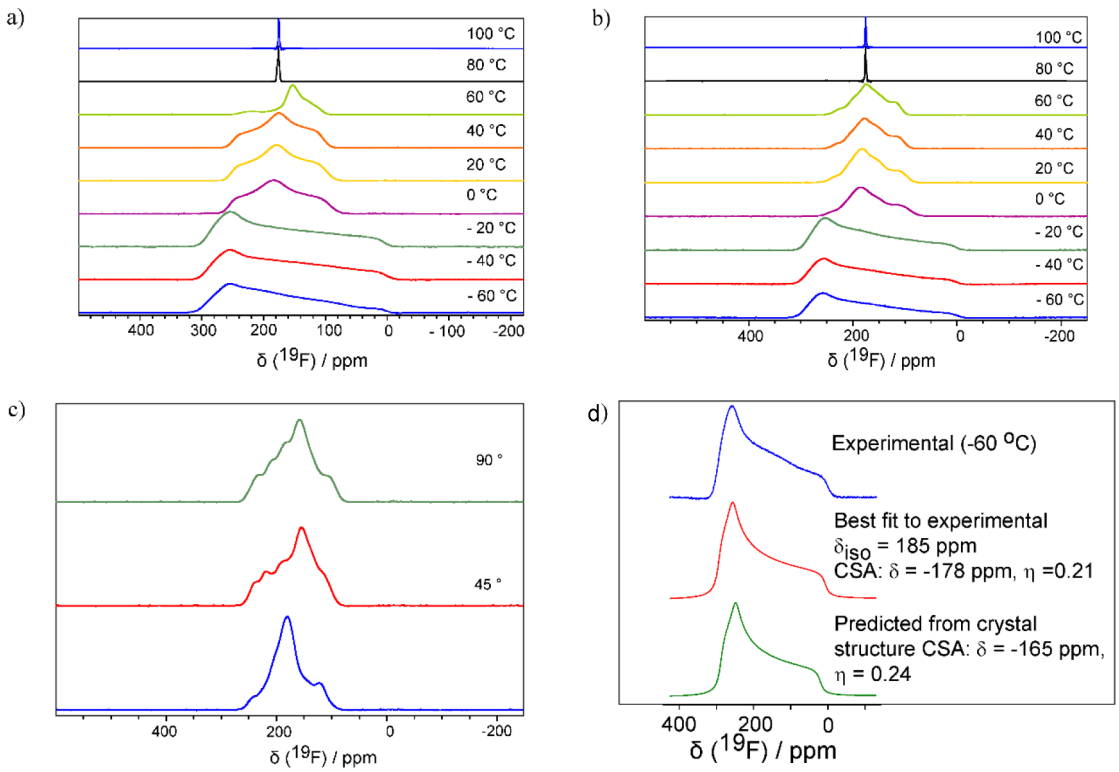

Figure 5. (a) Comparison of spin−echo ^{19}F NMR spectra recorded for [HMG][FSI] at different temperatures during heating followed by (b) cooling. (c) Spin−echo ^{19}F NMR after sample rotation inside the NMR probe by approximately 45 and 90° relative to the applied magnetic field at 20 °C. (d) ^{19}F CSA spectra and parameters predicted from the crystal structure against the experimental data recorded in phase III at −60 °C.

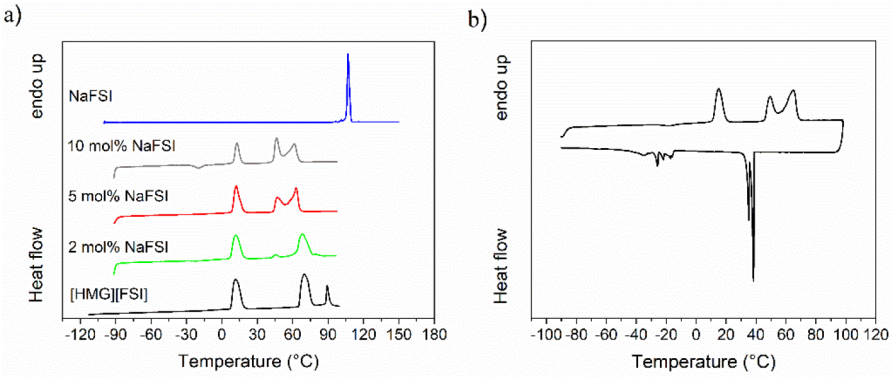

Figure 6. (a) DSC thermal traces of neat [HMG][FSI], 2, 5, and 10 mol % NaFSI in [HMG][FSI], and pure NaFSI. (b) Thermal phase behavior of a 5 mol % NaFSI mixture with OIPC recorded during the second heating and cooling cycle.

salt in OIPC), which promotes disorder and reduces the energy required to melt the sample.

Interestingly, for the 5 mol % NaFSI system, a complex series of solid−solid phase transitions that occur over a broader range of temperatures and consist of multiple peaks were also observed during the cooling process in the DSC experiment (Figures 6b and S1).

Ionic Conductivity. The temperature-dependent ionic conductivities of the neat [HMG][FSI] and binary mixture with 5 mol % NaFSI can be seen in Figure 7. Conductivity increasing with increasing temperature was observed for all of the values. Moreover, sodium salt addition to the neat [HMG][FSI] resulted in conductivities approximately an order of magnitude higher than for neat, as would be expected on the basis of some of the previously reported OIPC electrolyte systems.[38,40] The conductivity of neat [HMG][FSI] is 4.2 × 10^{-8} S cm^{-1} at 40 °C, whereas after the addition of 5 mol % NaFSI the conductivity increased by nearly 4 orders of magnitude to 2.1 × 10^{-4} S cm^{-1}. Conductivity values were reproducible, as confirmed after performing multiple heating and cooling scans on the samples.

Solid-State NMR Spectroscopy. The structural and dynamic behavior of the ions after sodium salt addition was investigated with solid-state NMR, where ^{1}H NMR was used to study the $[HMG]^{+}$ cation, ^{19}F was used to study the $[FSI]^{-}$ anion, and ^{23}Na was used to study the Na^{+} ions. Two different temperature programs were used to investigate the metastability and effects of solid−solid phase transitions (in particular, phase III to II) on the mobility and dynamics of the ions. Before each experiment, the sample cell was packed

https://doi.org/10.1021/acs.jpcc.1c01777
J. Phys. Chem. C XXXX, XXX, XXX−XXX

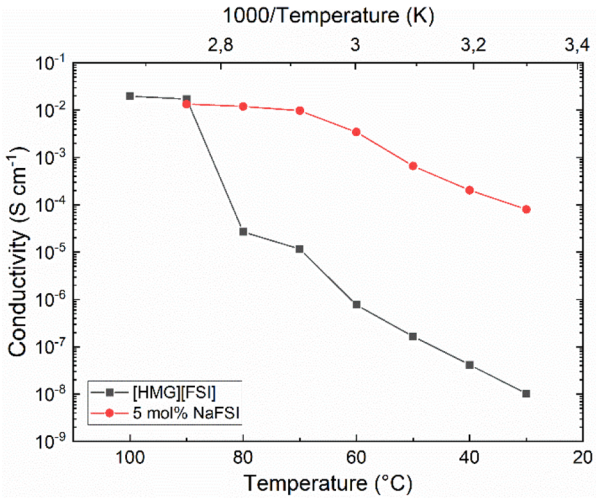

Figure 7. Ionic conductivity of neat [HMG][FSI] with 5 mol % NaFSI, measured using the same protocol where the sample was melted and cooled down to room temperature before measurement (EIS).

with a freshly prepared sample of electrolyte material inside an Ar-filled glovebox to ensure a consistent thermal history before each measurement. During the first experiment (experiment 1), the sample was heated from 30 to 80 °C, cooled, and then heated again, whereas in the second experiment (experiment 2), the sample was cooled to −40 °C and then heated to 80 °C. The thermal procedure applied in the second experiment allows the material to undergo the transition from phase III to II, which is not the case for the first experiment as the samples taken directly from the glovebox had been made by solvent casting at room temperature and had not been previously cooled to below room temperature.

The static NMR peak full width at half-maximum (fwhm) values for ^{23}Na and the spectra of ^{1}H and ^{19}F nuclei recorded during both experiments are presented in Figure 8a−d. Generally, narrower peaks are observed with increasing temperature, reflecting the increasing dynamics of the various ionic species. Moreover, a significant decrease in line widths as well as the appearance and growth of narrow components can be observed as material passes through solid−solid phase transitions.

The diffusivities of $[FSI]^-$ and $[HMG]^+$ in 5 mol % NaFSI in [HMG][FSI] samples were measured by pulsed field gradient nuclear magnetic resonance spectroscopy (PFG-NMR) and are presented in Figure 9. Unfortunately, the ^{19}F and ^{1}H spectra for the pure OIPC gave very weak signals due to fast T_2 relaxation, and thus their diffusion coefficients were not measurable. Rapid ^{23}Na relaxation also prevented the measurement of the Na^+ diffusivities. The temperature dependencies of diffusivity, shown in Figure 9, are characterized by the same trends for both ions, where increasing the temperature resulted in an increase in diffusivity. Interestingly, the anion diffusion coefficients are significantly higher (by nearly 2 orders of magnitude) than for the $[HMG]^+$ cation across the entire temperature range studied.

■ DISCUSSION

Detailed investigations using a combination of various analytical techniques, applied over different temperature programs, have shown a significant influence of thermal history and the formation of phase III on the material properties and ion dynamics for both the neat [HMG][FSI] and the 5 mol % NaFSI mixture. In the following text, we propose a model that can explain all of the experimental observations.

From the ionic conductivity of [HMG][FSI] measured by BDS, hysteresis was observed between cooling and heating through phase II. Moreover, a conductivity plateau was observed in phase II, which was also previously observed for other OIPCs.[41,42] Conductivity within one phase usually increases at a slower rate than the increase between different phases. This trend can be attributed to the difference in ion dynamics within a given phase and those initiated during a phase transition. The plateau within increasing temperature in phase II suggests an insignificant change in the number of diffusing ion species, although the rotational dynamics may increase. Interestingly, the observed conductivity was higher during the heating scan than during cooling. A potential explanation for this is that cooling down to −40 °C and creating phase III results in a structural transition and the creation of smaller crystal sizes and more grain boundaries, which would be expected to feature increased local disorder, dynamics, and free volume, thereby promoting ion transport. Upon heating, during the solid−solid phase transition from phase III to II some of these grain boundaries may remain in phase II after the transition, thereby explaining the higher conductivity in phase II on heating as opposed to cooling from the melt state where no residual effects of phase III are present.

This behavior is also consistent with the thermal phase behavior where the transition from phase III to II does not appear to be fully reversible as the cooling curve shows evidence of sluggish crystallization involving multiple overlapping peaks. This complex crystallization process may be attributed to multiple freezing processes and the formation of numerous small crystallites.

This model is also consistent with the trend observed in the SXRD patterns where the number of diffraction peaks decreased with increasing temperature, which is usually related to an increase in the symmetry. A possible explanation is that at a higher temperature, the degree of disorder in the crystal structure increases. This is very likely caused by an increase in the degree of rotational motion of the molecules through the phase transition and the drastic increase in molecular mobility. Moreover, SXRD showed different crystal structures for each of the [HMG][FSI] phases.

The effect of phase III creation on crystallite sizes and ion dynamics was also observed during solid-state NMR experiments, where different ^{19}F powder pattern shapes were recorded in phase II during heating compared to cooling after melting. For the heating run, the sample was first cooled to −60 °C, which resulted in phase III. As we can see from Figure 5a, during the heating cycle classic CSA patterns were observed in phase II, whereas on cooling (Figure 5b) the line shapes depart from the "ideal" CSA pattern shape. To examine the reproducibility of this behavior, this experiment was performed multiple times. Interestingly, during heating the classic CSA pattern was always observed, whereas on cooling the ^{19}F line shape was different each time. This behavior can be attributed to larger crystallite sizes, resulting in some preferential orientation, a phenomenon which was also previously observed in other OIPCs.[43,44] To confirm the presence of preferential crystal orientations, the sample was cooled from the melt and physically rotated inside the NMR

https://doi.org/10.1021/acs.jpcc.1c01777
J. Phys. Chem. C XXXX, XXX, XXX−XXX

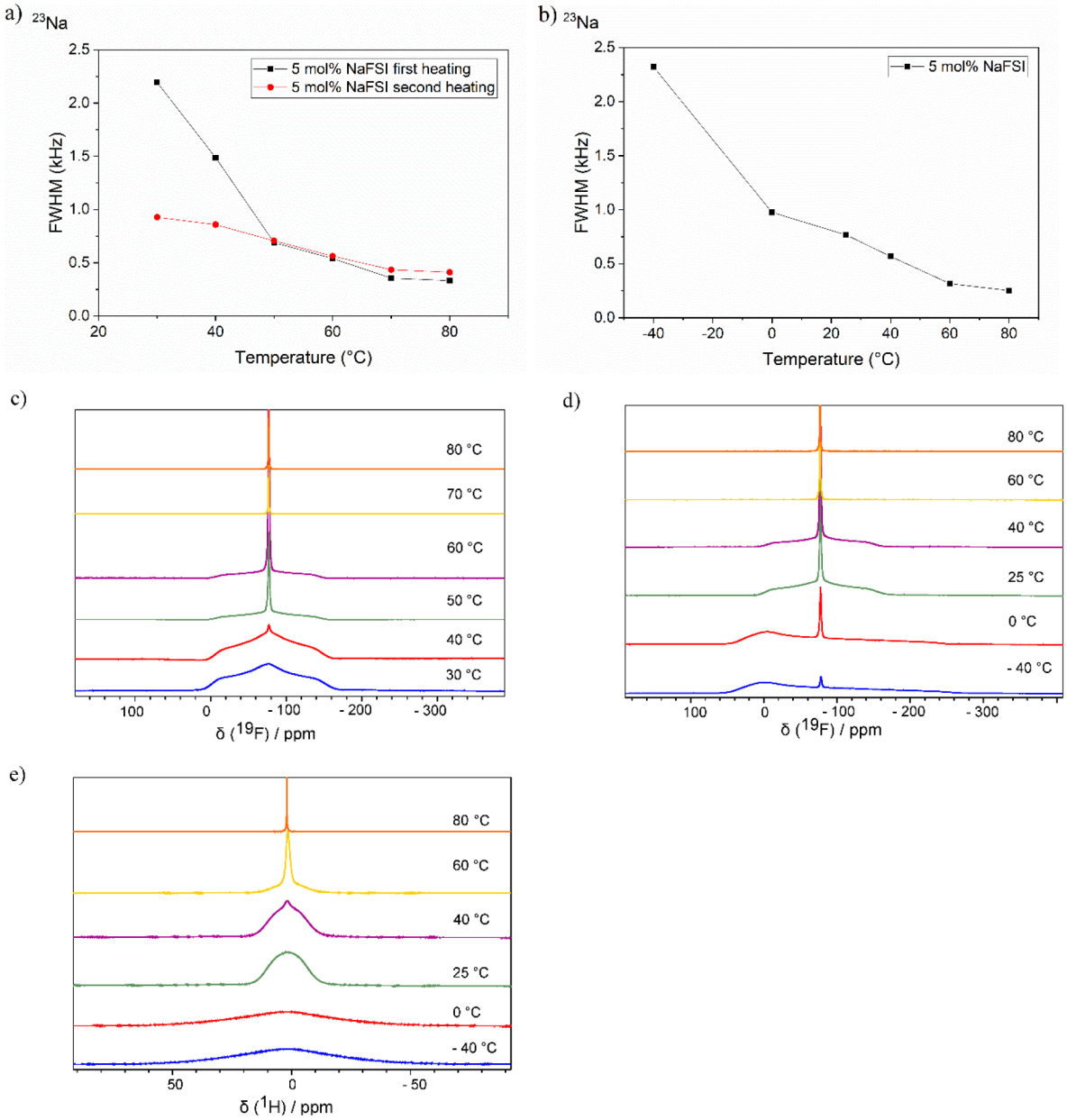

Figure 8. (a) Comparison of the full width at half maximum (fwhm) of the ^{23}Na NMR spectra as a function of the temperature of 5 mol % NaFSI in [HMG][FSI] during two heating cycles (30−80 °C) obtained from experiment 1 and (b) during heating from −40 to 80 °C from experiment 2. Evolution of spin−echo ^{19}F spectra versus the temperature of 5 mol % NaFSI recorded during (c) experiment 1 and (d) experiment 2. (e) ^{1}H spectral line widths: stack spectra of 5 mol % NaFSI in [HMG][FSI] recorded at various temperatures during the first heating scan.

probe by approximately 45 and 90° relative to the applied magnetic field. Figure 5c shows ^{19}F spin echo spectra recorded before and after rotation, where differences in the pattern can be observed. This would not be observed if the orientations of the anions (or crystallites) were isotropically distributed and therefore confirms that the crystallite orientations are anisotropic, presumably dependent on the orientations of the first crystals that nucleate during the cooling.

Such orientation effects are more likely to be observed for larger crystallite sizes and therefore fewer grain boundaries. These observations back up our proposed explanation for the hysteresis seen in the conductivity measurements as discussed above. It should also be noted that the conductivity dependence on preferential orientation will be determined by the conductivity mechanism, which in this case is assumed to occur via the grain boundaries and through vacancies in the bulk crystals. In the case of [HMG][FSI], this preferential orientation appears to decrease the ionic conductivity, likely because of larger crystal sizes and fewer grain boundaries present as a result. On the other hand, cooling the material to crystallize phase III results in a return to a more homogeneous sample with smaller crystallites. An analogous trend was reported by Romanenko et al., who observed crystallization to a new crystal structure and the disappearance of the preferential alignment as [P_{1i444}][FSI] passed through a solid−solid phase transition.[44]

Similar thermal phase behavior, where a sluggish and complex solid−solid phase transition was recorded for the

https://doi.org/10.1021/acs.jpcc.1c01777
J. Phys. Chem. C XXXX, XXX, XXX−XXX

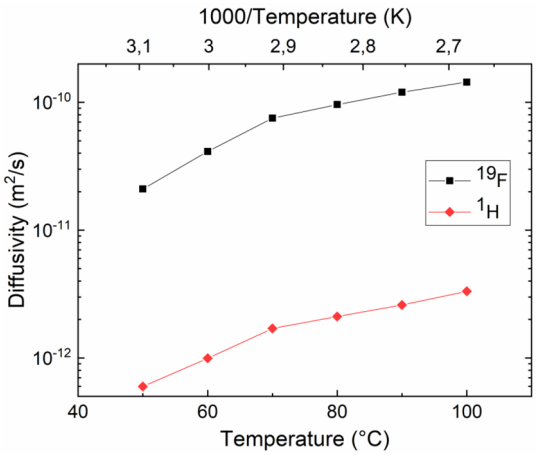

Figure 9. Diffusivities (D) of $[FSI]^-$ and $[HMG]^+$ measured for 5 mol % NaFSI in [HMG][FSI] using PFG NMR as a function of temperature.

neat OIPC, was also observed on the cooling scan during DSC analysis of the mixture with NaFSI (Figure 6b). Moreover, the effect of the thermal history and phase III creation on the ion mobility was also observed for the 5 mol % NaFSI in [HMG][FSI].

From two different solid-state NMR experiments performed, where during the first (experiment 1) the sample was heated twice from 30 to 80 °C and in the second (experiment 2) the material was cooled to −40 °C followed by heating to 80 °C, the effect of phase III can be seen. Interestingly, during the second temperature program (experiment 2, Figure 8b), where the sample was first cooled to −40 °C (phase III) and then heated, a significantly narrower fwhm was observed for ^{23}Na (i.e., more mobile Na^+) in phase II than the one observed during the first heating cycle in experiment 1 (starting from room temperature). These results together with the ionic conductivity data of the pure OIPC confirm that cooling the samples into phase III leads to a higher mobility of Na ions and increased total ionic conductivity compared to the conductivity obtained from the measurement which starts from 30 °C. The improved ionic conductivity can be attributed to the phase III restructuring and formation of smaller crystal sizes, resulting in more grain boundaries in phase III that can provide fast ion pathways through the material.

An analogous effect of the creation of phase III on the ion mobility was also observed in the ^{19}F and ^{1}H spectra (Figure 8c−e). Figure 8c shows the spin−echo ^{19}F spectra evolution with increasing temperature recorded during the first heating cycle, while the results of the prior cooling of the sample during the second temperature program are presented in Figure 8d. A comparison of spectra recorded at 25 or 30 and 40 °C presented in both figures leads to the consistent conclusion that the creation of phase III has a strong impact on the mobility of the ions. Moreover, the recorded spectra consist of two components: one narrow peak which corresponds to an anion undergoing isotropic rotation (and potentially also translational mobility), presumably in the disordered grain boundary region, and the other a broad peak which corresponds to an immobile anion within the bulk crystal structure. A significantly higher fraction of the mobile component is presented at ambient temperature during the second experiment, in which material was cooled to −40 °C, than in the measurement performed at 25 °C. Moreover, the spectral line shape is remarkably different in phase III, suggesting different $[FSI]^-$ dynamics which change as the material undergoes the transition from phase III to II.

Interestingly, whereas for ^{23}Na and ^{19}F a significant increase in mobile Na^+ and $[FSI]^-$ species in phase III was observed as the material was cooled to −40 °C (compared to phase II), this is not the case for the ^{1}H spectra where no mobile fraction can be seen in phase III and peak narrowing is observed only after the material undergoes the transition to phase II. This remarkable observation, where a different temperature dependence is observed for the cation and anion, suggests decoupled ion dynamics and is analogous to previously reported findings for diethyl(methyl)(isobutyl)phosphonium hexafluorophosphate ($[P_{1,2,2,4}][PF_6]$).[3,45]

Additionally, the measured anion diffusion coefficients are significantly higher than those of the cation. Usually, in the majority of IL and OIPC systems studied, anions have a relatively similar diffusion, at least within the same order of magnitude. For example, similar diffusivities of both ^{1}H and ^{19}F were observed in 5 mol % $[C_3mpyr][FSI]$/NaFSI IL, reported as 10^{-11} m^2/s (estimated graphically).[46] This unusual behavior may be partially attributable to the smaller size of the $[FSI]^-$ ions versus the larger $[HMG]^+$. However, the almost 2 orders of magnitude difference is unlikely to be due to size alone. Moreover, strong ion decoupling was not previously observed for [HMG][FSI] with LiFSI/LiTFSI reported systems. The proton diffusion coefficient in 10 mol % LiFSI in [HMG]FSI] is 2.6×10^{-11} m^2/s whereas ^{19}F diffusivity is 3.4×10^{-11} m^2/s at 50 °C. It is possible that the $[HMG]^+$ cations self-assemble through cation−cation interactions in a way that causes a much lower diffusivity compared to the $[FSI]^-$ anions, and this is consistent with the decoupled ion dynamics also observed from the solid-state NMR data. If the Na^+ cation is moving with $[FSI]^-$, then one may expect it to be quite diffusive. However, this hypothesis needs to be confirmed by further experiments in the future.

Furthermore, during experiment 1 (a 5 mol % NaFSI sample heated twice from 30 to 80 °C) the Na^+ mobility is significantly higher at 30 °C during the second heating scan, which can be seen from the lower fwhm values in Figure 8a. This suggests that the sample is not fully crystallized during cooling to 30 °C, and there is some fraction of a metastable phase remaining that results in higher ion mobility. This trend was consistent for all nuclei recorded during experiment 1, where the supercooling effect arising from sample metastability has a significant effect. After melting the sample, the material needs more energy to fully recrystallize than is available to overcome the slow rearrangement of the ions which are therefore trapped in a metastable (high-energy) state. This can be seen here from the difference between the ^{1}H spectra recorded during the first (SI Figure 3a) and second (SI Figure 3b) heating scans where a significantly larger amount of the mobile component was observed during the second heating. Metastable behavior is well known for OIPC-based electrolytes and has previously been reported in the literature.[4,18,40]

■ CONCLUSIONS

The thermal phase behavior and ion mobility in the neat OIPC [HMG][FSI] and a binary mixture with NaFSI were studied for the first time. Unusual conductivity behavior of [HMG]-[FSI] was reported, where interestingly it was observed to be higher during a heating cycle (from −40 °C) than during a cooling cycle, which is not typically observed for OIPCs. This

https://doi.org/10.1021/acs.jpcc.1c01777
J. Phys. Chem. C XXXX, XXX, XXX−XXX

behavior can be attributed to the larger number of grain boundaries created in phase III during a complex crystallization process, as observed in the DSC analysis. We propose that these disordered grain boundaries remain in phase II after the solid−solid phase transition from phase III to II, leading to the higher conductivity in phase II than is observed after cooling from the melt. Furthermore, a similar trend was observed for the 5 mol % NaFSI in the [HMG][FSI] electrolyte where the sodium mobility recorded during the solid-state NMR experiment was higher after cooling the material sufficiently to create phase III vs conductivity measured during the experiment starting from 30 °C. Despite changes in the thermal phase behavior when adding the sodium salt to the neat [HMG][FSI], where a new peak appears and the solid−solid phase transition overlaps with the melting peak, a similarity in the dependence of ion dynamics on thermal history was observed. Moreover, the new peak observed at 44 °C was recorded after 2 mol % sodium salt addition and was observed to grow with increasing NaFSI concentration, which may be attributed to a eutectic transition. However, to confirm this hypothesis, more electrolyte concentrations need to be prepared and examined.

The effect of the formation of phase III on the ion dynamics was also seen from changes in the ^{19}F solid-state NMR line shape, where the preferential crystallite orientation was confirmed by sample rotation. Furthermore, the calculation of ^{19}F chemical shielding anisotropy (CSA) parameters from the crystal structure showed good agreement with the experimental data, which confirms the accuracy of the crystal structure.

Finally, ion decoupling in the 5 mol % NaFSI sample observed from PFG-NMR studies was consistent with solid-state NMR results where, despite changes in the ^{23}Na and ^{19}F spectra depending on the temperature program used, the ^{1}H spectra remained unchanged. This is in contrast to the same OIPC mixed with Li salts reported previously, where all ions were found to diffuse at similar rates.[26]

This work illustrates the potential complexity of phase behavior in OIPCs and the importance of thermal history in determining the ion mobility and ionic conductivity. An improved understanding of how material properties depend on such external parameters will allow us to enhance the electrolyte performance. In the case of [HMG][FSI], cooling the material and creating phase III results in higher conductivity and also higher Na mobility for the 5 mol % NaFSI electrolyte.

■ ASSOCIATED CONTENT

Supporting Information

The Supporting Information is available free of charge at https://pubs.acs.org/doi/10.1021/acs.jpcc.1c01777.

DSC thermal traces of 5 mol % NaFSI in [HMG][FSI] recorded during the first scan and second heating scan; the first scan was used to remove the thermal history and is not reported in the main text; details of SXRD refinement, showing the evolution of the cell volume over temperature which follows Vegard's law; and electrolyte metastability and a supercooling effect resulting in a difference between the ^{1}H spectra recorded during two heating cycles (PDF)

■ AUTHOR INFORMATION

Corresponding Author

Maria Forsyth − *ARC Centre of Excellence for Electromaterials Science (ACES), Institute for Frontier Materials (IFM), Deakin University, Burwood, Victoria 3125, Australia;* orcid.org/0000-0002-4273-8105; Email: maria.forsyth@deakin.edu.au

Authors

Karolina Biernacka − *ARC Centre of Excellence for Electromaterials Science (ACES), Institute for Frontier Materials (IFM), Deakin University, Burwood, Victoria 3125, Australia;* orcid.org/0000-0002-4124-1850

Faezeh Makhlooghiazad − *ARC Centre of Excellence for Electromaterials Science (ACES), Institute for Frontier Materials (IFM), Deakin University, Burwood, Victoria 3125, Australia*

Ivan Popov − *Chemical Sciences Division, Oak Ridge National Laboratory, Oak Ridge, Tennessee 37831, United States*

Haijin Zhu − *Institute for Frontier Materials and the ARC Centre of Excellence for Electromaterials Science, Deakin University, Geelong, Victoria 3216, Australia*

Jean-Noël Chotard − *Laboratoire de Réactivité et de Chimie des Solides (LRCS), CNRS UMR 7314, Université de Picardie Jules Verne, 80039 Amiens Cedex, France;* orcid.org/0000-0002-9867-7954

Craig M. Forsyth − *School of Chemistry, Monash University, Clayton, Victoria 3800, Australia*

Ruhamah Yunis − *Centre for Materials Science, Queensland University of Technology (QUT), Brisbane, QLD 4000, Australia*

Luke A. O'Dell − *Institute for Frontier Materials and the ARC Centre of Excellence for Electromaterials Science, Deakin University, Geelong, Victoria 3216, Australia;* orcid.org/0000-0002-7760-5417

Alexei P. Sokolov − *Chemical Sciences Division, Oak Ridge National Laboratory, Oak Ridge, Tennessee 37831, United States; Department of Chemistry, University of Tennessee, Knoxville, Tennessee 37996, United States;* orcid.org/0000-0002-8187-9445

Jennifer M. Pringle − *ARC Centre of Excellence for Electromaterials Science (ACES), Institute for Frontier Materials (IFM), Deakin University, Burwood, Victoria 3125, Australia*

Complete contact information is available at: https://pubs.acs.org/10.1021/acs.jpcc.1c01777

Notes

The authors declare no competing financial interest.

■ ACKNOWLEDGMENTS

This work was financially supported by the Australian Research Council through the ARC Centre of Excellence for Electromaterials Science (grant no. CE140100012). The U.S. team acknowledges NSF support (award CHE-1764409) for dielectric measurements.

■ REFERENCES

(1) Mauger, A.; Julien, C. M.; Goodenough, J. B.; Zaghib, K. Tribute to Michel Armand: From Rocking Chair − Li-Ion to Solid-State Lithium Batteries. *J. Electrochem. Soc.* **2020**, *167*, 070507.

(2) Lebedeva, N. P.; Boon-Brett, L. Considerations on the Chemical Toxicity of Contemporary Li-Ion Battery Electrolytes and Their Components. *J. Electrochem. Soc.* **2016**, *163*, A821−A830.

(3) Zhu, H.; MacFarlane, D. R.; Pringle, J. M.; Forsyth, M. Organic Ionic Plastic Crystals as Solid-State Electrolytes. *Trends Chem.* **2019**, *1*, 126−140.

(4) Pringle, J. M. Recent Progress in the Development and Use of Organic Ionic Plastic Crystal Electrolytes. *Phys. Chem. Chem. Phys.* **2013**, *15*, 1339−1351.

(5) Armel, V.; Forsyth, M.; MacFarlane, D. R.; Pringle, J. M. Organic Ionic Plastic Crystal Electrolytes; a New Class of Electrolyte for High Efficiency Solid State Dye-Sensitized Solar Cells. *Energy Environ. Sci.* **2011**, *4*, 2234.

(6) Jin, L.; Nairn, K. M.; Forsyth, C. M.; Seeber, A. J.; MacFarlane, D. R.; Howlett, P. C.; Forsyth, M.; Pringle, J. M. Structure and Transport Properties of a Plastic Crystal Ion Conductor: Diethyl-(Methyl)(Isobutyl)Phosphonium Hexafluorophosphate. *J. Am. Chem. Soc.* **2012**, *134*, 9688−9697.

(7) Pringle, J. M.; Howlett, P. C.; MacFarlane, D. R.; Forsyth, M. Organic Ionic Plastic Crystals: Recent Advances. *J. Mater. Chem.* **2010**, *20*, 2056.

(8) Huang, J.; Hill, A.; Forsyth, M.; MacFarlane, D.; Hollenkamp, A. Conduction in Ionic Organic Plastic Crystals: The Role of Defects. *Solid State Ionics* **2006**, *177*, 2569−2573.

(9) Zhou, Z.; Bin; Matsumoto, H. Lithium-Doped, Organic Ionic Plastic Crystal Electrolytes Exhibiting High Ambient-Temperature Conductivities. *Electrochem. Commun.* **2007**, *9*, 1017−1022.

(10) Jin, L.; Howlett, P.; Efthimiadis, J.; Kar, M.; MacFarlane, D.; Forsyth, M. Lithium Doped N,N-Dimethyl Pyrrolidinium Tetrafluoroborate Organic Ionic Plastic Crystal Electrolytes for Solid State Lithium Batteries. *J. Mater. Chem.* **2011**, *21*, 10171−10178.

(11) Macfarlane, D. R.; Huang, J.; Forsyth, M. Lithium-Doped Plastic Crystal Electrolytes Exhibiting Fast Ion Conduction for Secondary Batteries. *Nature* **1999**, *402*, 792−794.

(12) Jin, L.; Nairn, K. M.; Ling, C. D.; Zhu, H.; O'Dell, L. A.; Li, J.; Chen, F.; Pavan, A. F.; Madsen, L. A.; Howlett, P. C.; Macfarlane, D. R.; Forsyth, M.; Pringle, J. M. Conformational Dynamics in an Organic Ionic Plastic Crystal. *J. Phys. Chem. B* **2017**, *121*, 5439−5446.

(13) Forsyth, M.; Chimdi, T.; Seeber, A.; Gunzelmann, D.; Howlett, P. C. Structure and Dynamics in an Organic Ionic Plastic Crystal, N-Ethyl-N-Methyl Pyrrolidinium Bis(Trifluoromethanesulfonyl) Amide, Mixed with a Sodium Salt. *J. Mater. Chem. A* **2014**, *2*, 3993−4003.

(14) Henderson, W. A.; Seo, D. M.; Zhou, Q.; Boyle, P. D.; Shin, J. H.; De Long, H. C.; Trulove, P. C.; Passerini, S. An Alternative Ionic Conductivity Mechanism for Plastic Crystalline Salt-Lithium Salt Electrolyte Mixtures. *Adv. Energy Mater.* **2012**, *2*, 1343−1350.

(15) Forsyth, M.; Chimdi, T.; Seeber, A.; Gunzelmann, D.; Howlett, P. C. Structure and Dynamics in an Organic Ionic Plastic Crystal, N-Ethyl-N-Methyl Pyrrolidinium Bis(Trifluoromethanesulfonyl) Amide, Mixed with a Sodium Salt. *J. Mater. Chem. A* **2014**, *2*, 3993−4003.

(16) Chimdi, T.; Gunzelmann, D.; Vongsvivut, J.; Forsyth, M. A Study of Phase Behavior and Conductivity of Mixtures of the Organic Ionic Plastic Crystal N-Methyl-N-Methyl-Pyrrolidinium Dicyanamide with Sodium Dicyanamide. *Solid State Ionics* **2015**, *272*, 74−83.

(17) Makhlooghiazad, F.; Gunzelmann, D.; Hilder, M.; MacFarlane, D. R.; Armand, M.; Howlett, P. C.; Forsyth, M. Mixed Phase Solid-State Plastic Crystal Electrolytes Based on a Phosphonium Cation for Sodium Devices. *Adv. Energy Mater.* **2017**, *7*, 1601272.

(18) Makhlooghiazad, F.; Howlett, P. C.; Wang, X.; Hilder, M.; MacFarlane, D. R.; Armand, M.; Forsyth, M. Phosphonium Plastic Crystal Salt Alloyed with a Sodium Salt as a Solid-State Electrolyte for Sodium Devices: Phase Behaviour and Electrochemical Performance. *J. Mater. Chem. A* **2017**, *5*, 5770−5780.

(19) Makhlooghiazad, F.; Yunis, R.; Mecerreyes, D.; Armand, M.; Howlett, P. C.; Forsyth, M. Comparison of the Physicochemical and Electrochemical Behaviour of Mixed Anion Phosphonium Based OIPCs Electrolytes for Sodium Batteries. *Solid State Ionics* **2017**, *312*, 44−52.

(20) Yang, H.; Hwang, J.; Wang, Y.; Matsumoto, K.; Hagiwara, R. N-Ethyl- N-Propylpyrrolidinium Bis(Fluorosulfonyl)Amide Ionic Liquid Electrolytes for Sodium Secondary Batteries: Effects of Na Ion Concentration. *J. Phys. Chem. C* **2019**, *123*, 22018−22026.

(21) Makhlooghiazad, F.; Guazzagaloppa, J.; O'Dell, L. A.; Yunis, R.; Basile, A.; Howlett, P. C.; Forsyth, M. The Influence of the Size and Symmetry of Cations and Anions on the Physicochemical Behavior of Organic Ionic Plastic Crystal Electrolytes Mixed with Sodium Salts. *Phys. Chem. Chem. Phys.* **2018**, *20*, 4721−4731.

(22) Al-Masri, D.; Yunis, R.; Hollenkamp, A. F.; Doherty, C. M.; Pringle, J. M. The Influence of Alkyl Chain Branching on the Properties of Pyrrolidinium-Based Ionic Electrolytes. *Phys. Chem. Chem. Phys.* **2020**, *22*, 18102−18113.

(23) Yunis, R.; Pringle, J. M.; Wang, X.; Girard, G. M. A.; Kerr, R.; Zhu, H.; Howlett, P. C.; Macfarlane, D. R.; Forsyth, M. Solid (Cyanomethyl)Trimethylammonium Salts for Electrochemically Stable Electrolytes for Lithium Metal Batteries. *J. Mater. Chem. A* **2020**, *8*, 14721−14735.

(24) Yunis, R.; Newbegin, T. W.; Hollenkamp, A. F.; Pringle, J. M. Ionic Liquids and Plastic Crystals with a Symmetrical Pyrrolidinium Cation. *Mater. Chem. Front.* **2018**, *2*, 1207−1214.

(25) Yunis, R.; Al-Masri, D.; Hollenkamp, A. F.; Doherty, C. M.; Zhu, H.; Pringle, J. M. Plastic Crystals Utilising Small Ammonium Cations and Sulfonylimide Anions as Electrolytes for Lithium Batteries. *J. Electrochem. Soc.* **2020**, *167*, 070529.

(26) Biernacka, K.; Al-Masri, D.; Yunis, R.; Zhu, H.; Hollenkamp, A. F.; Pringle, J. M. Development of New Solid-State Electrolytes Based on a Hexamethylguanidinium Plastic Crystal and Lithium Salts. *Electrochim. Acta* **2020**, *357*, 136863.

(27) Yunis, R.; Hollenkamp, A. F.; Forsyth, C.; Doherty, C. M.; Al-Masri, D.; Pringle, J. M. Organic Salts Utilising the Hexamethylguanidinium Cation: The Influence of the Anion on the Structural, Physical and Thermal Properties. *Phys. Chem. Chem. Phys.* **2019**, *21*, 12288−12300.

(28) Al-Masri, D.; Yunis, R.; Hollenkamp, A. F.; Pringle, J. M. A Symmetrical Ionic Liquid/Li Salt System for Rapid Ion Transport and Stable Lithium Electrochemistry. *Chem. Commun.* **2018**, *54*, 3660−3663.

(29) Boultif, A.; Louer, D. Powder Pattern Indexing with the Dichotomy Method. *J. Appl. Crystallogr.* **2004**, *37*, 724−731.

(30) Rodríguez-Carvajal, J. Recent Developments of the Program FULLPROF. *Comm. Powder Diffr.* **2001**, *26*, 12−19.

(31) Rodríguez-Carvajal, J. Recent Advances in Magnetic Structure Determination by Neutron Powder Diffraction. *Phys. B* **1993**, *192*, 55−69.

(32) CrysAlis PRO. Rigaku Oxford Diffraction. *Yarnton, England,* 2019.

(33) Sheldrick, G. M. Crystal Structure Refinement with SHELXL. *Acta Crystallogr., Sect. C: Struct. Chem.* **2015**, *71*, 3−8.

(34) Clark, S. J.; Segall, M. D.; Pickard, C. J.; Hasnip, P. J.; Probert, M. I. J.; Refson, K.; Payne, M. C. First Principles Methods Using CASTEP. *Z. Kristallogr. - Cryst. Mater.* **2005**, *220*, 567−570.

(35) Abu-Lebdeh, Y.; Alarco, P. J.; Abouimrane, A.; Ionescu-Vasii, L.; Hammami, A.; Armand, M. A Single-Phased Ringed Pyrazolium Imide and Its Potential Application for Plastic Crystal-Lithium Batteries. *J. New Mater. Electrochem. Syst.* **2005**, *8*, 197−201.

(36) Timmermans, J. Plastic Crystals: A Historical Review. *J. Phys. Chem. Solids* **1961**, *18*, 1−8.

(37) Denton, A. R.; Ashcroft, N. W. Vegard's "Law. *Phys. Rev. A: At., Mol., Opt. Phys.* **1991**, *43*, 3161−3164.

(38) Jin, L.; Howlett, P. C.; Pringle, J. M.; Janikowski, J.; Armand, M.; MacFarlane, D. R.; Forsyth, M. An Organic Ionic Plastic Crystal Electrolyte for Rate Capability and Stability of Ambient Temperature Lithium Batteries. *Energy Environ. Sci.* **2014**, *7*, 3352−3361.

(39) Abu-Lebdeh, Y.; Alarco, P. J.; Armand, M. Conductive Organic Plastic Crystals Based on Pyrazolium Imides. *Angew. Chem., Int. Ed.* **2003**, *42*, 4499−4501.

(40) Iranipour, N.; Gunzelmann, D. J.; Seeber, A. J.; Vongsvivut, J.; Hollenkamp, A. F.; Forsyth, M.; Howlett, P. C. Effect of Secondary

https://doi.org/10.1021/acs.jpcc.1c01777
J. Phys. Chem. C XXXX, XXX, XXX−XXX

Phase on Thermal Behaviour and Solid-State Ion Conduction in Lithium Doped N-Ethyl-N-Methylpyrrolidinium Tetrafluoroborate Organic Ionic Plastic Crystal. *J. Mater. Chem. A* **2017**, *5*, 24909−24919.

(41) Armel, V.; Velayutham, D.; Sun, J.; Howlett, P. C.; Forsyth, M.; MacFarlane, D. R.; Pringle, J. M. Ionic Liquids and Organic Ionic Plastic Crystals Utilizing Small Phosphonium Cations. *J. Mater. Chem.* **2011**, *21*, 7640−7650.

(42) Yunis, R.; Al-Masri, D.; Hollenkamp, A. F.; Doherty, C. M.; Zhu, H.; Pringle, J. M. Plastic Crystals Utilising Small Ammonium Cations and Sulfonylimide Anions as Electrolytes for Lithium Batteries. *J. Electrochem. Soc.* **2020**, *167*, 070529.

(43) Romanenko, K.; Jin, L.; Madsen, L. A.; Pringle, J. M.; Odell, L. A.; Forsyth, M. Anisotropic MRI Contrast Reveals Enhanced Ionic Transport in Plastic Crystals. *J. Am. Chem. Soc.* **2014**, *136*, 15638−15645.

(44) Romanenko, K.; Pringle, J. M.; O'Dell, L. A.; Forsyth, M. New Insights into the Thermal Behaviour of Organic Ionic Plastic Crystals: Magnetic Resonance Imaging of Polycrystalline Morphology Alterations Induced by Solid-Solid Phase Transitions. *Phys. Chem. Chem. Phys.* **2015**, *17*, 18991−19000.

(45) Chen, F.; Jin, L.; De Leeuw, S. W.; Pringle, J. M.; Forsyth, M. Atomistic Simulation of Structure and Dynamics of the Plastic Crystal Diethyl(Methyl)(Isobutyl)Phosphonium Hexafluorophosphate. *J. Chem. Phys.* **2013**, *138*, 244503.

(46) Forsyth, M.; Yoon, H.; Chen, F.; Zhu, H.; MacFarlane, D. R.; Armand, M.; Howlett, P. C. Novel Na+Ion Diffusion Mechanism in Mixed Organic-Inorganic Ionic Liquid Electrolyte Leading to High Na+Transference Number and Stable, High Rate Electrochemical Cycling of Sodium Cells. *J. Phys. Chem. C* **2016**, *120*, 4276−4286.

https://doi.org/10.1021/acs.jpcc.1c01777
J. Phys. Chem. C XXXX, XXX, XXX−XXX